

A new transient bioheat model of the human body and its integration to clothing models

M. Salloum^a, N. Ghaddar^{a,*}, K. Ghali^b

^a Department of Mechanical Engineering, American University of Beirut, PO Box 11-0236, Beirut 1107-2020, Lebanon

^b Department of Mechanical Engineering, Beirut Arab University, Beirut, Lebanon

Received 23 August 2005; received in revised form 1 June 2006; accepted 26 June 2006

Available online 27 October 2006

Abstract

A mathematical multi-segmented model based on an improved Stolwijk model is developed for predicting nude human thermal and regulatory responses within body segments and the environment. The passive model segments the body into the 15 cylindrical segments. Each body segment is divided into four nodes of core, skin, artery blood, and vein blood. In any body element, the blood exiting the arteries and flowing into the capillaries is divided into blood flowing in the core (exchanges heat by perfusion in the core) and blood flowing into the skin layer (exchanges heat by perfusion in the skin). The model calculates the blood circulation flow rates based on exact physiological data of Avolio [A.P. Avolio, Multi-branched model of the human arterial system, *Med. Biol. Eng. Comp.* 18 (1980) 709–718] and real dimensions and anatomic positions of the arteries in the body. The inclusion of calculated blood perfusion in the tissue is based on the pulsating arterial system model and the heart rate is unique for the current model. The nude body model is integrated to an existing clothing model based on heat and mass diffusion through the clothing layers and takes into consideration the moisture adsorption by the fibers. The bioheat human model is capable of predicting accurately nude human transient physiological responses such as the body's skin, tympanic, and core temperatures, sweat rates, and the dry and latent heat losses from each body segment.

The nude and clothed body models predictions are compared with published experimental data at a variety of ambient conditions and activity. The current model agrees well with experimental data during transitions from hot to cold environments and during changes in metabolic rate. Both the nude and clothed human model have an accuracy of less than 8% for the whole-body heat gains or losses; the nude human model has an accuracy of ± 0.48 °C for skin temperature values.

© 2006 Elsevier Masson SAS. All rights reserved.

1. Introduction

Mathematical modeling of the human body thermal response is a valuable tool to understand the human body thermal behavior under different environmental conditions and activity levels. Bioheat models are needed in a variety of applications and have been successfully used [2] in thermal comfort research aimed for energy efficiency, and human thermal discomfort under exposure to extreme hot or cold conditions as in fire fighting or deep sea diving [3]. The continuing rise in energy demand resulted in the need for designing energy efficient HVAC systems for thermal comfort in transient and steady state conditions. The

prediction of the human thermal response in transient or steady non-uniform environment can benefit from the development of a realistic bioheat model [4–6]. In such applications, it has been necessary to build thermal models of the human body that are able to predict core and partitional body temperatures during time transients in any environment. The single-segment and multi-segmental models for the human body and its thermoregulatory responses have been developed based on the theories of physiology, thermodynamics and transport processes for the prediction of thermal behavior of either the entire human body or a part of it [4,7–11].

Gagge developed a simple and an easy-to-implement one-segment two-layer (core and skin) lumped model of the human body [7,12]. Gagge derived energy balances for the core and the skin. The control system equations were written as a function of temperature signals for shivering, sudomotor response

* Corresponding author. Tel.: +961 1 350000 ext 3494; fax: +961 1 744462.
E-mail address: farah@aub.edu.lb (N. Ghaddar).

Nomenclature

A	area	m^2	$R_{d, \text{fab}}$	fabric dry resistance	$\text{m}^2 \text{K W}^{-1}$
a_j	artery vessel branch number		R_e	combined air-clothing layer evaporative resistance	$\text{m}^2 \text{kPa W}^{-1}$
C	thermal capacitance	J K^{-1}	$R_{e, \text{fab}}$	fabric evaporative resistance	$\text{m}^2 \text{kPa W}^{-1}$
c	specific heat	$\text{J kg}^{-1} \text{K}^{-1}$	t	time	s
CO	Cardiac output	$\text{cm}^3 \text{hr}^{-1}$	T	temperature	$^{\circ}\text{C}$
e_{fab}	fabric thickness	m	<i>Greek symbol</i>		
$h(t)$	pulsating blood flow convective heat transfer coefficient	$\text{W m}^{-2} \text{K}^{-1}$	ρ	density	kg m^{-3}
h_{mean}	mean non-pulsating blood flow convection coefficient	$\text{W m}^{-2} \text{K}^{-1}$	<i>Subscripts</i>		
I_{sk}	skin evaporative resistance	$\text{m}^2 \text{kPa W}^{-1}$	a	artery	
$I_{\text{a-sk}}$	evaporative resistance of air layer adjacent	$\text{m}^2 \text{kPa W}^{-1}$	bl	blood	
K	conductance	W K^{-1}	bl, a	artery blood	
L	water latent heat of vaporization	J kg^{-1}	bl, v	vein blood	
M	segmental metabolic rate	W	C	convective	
M_{basal}	thermoneutrality metabolic rate	W	co	constricted	
M_{total}	total metabolic rate	W	cr	core	
W	external work	W	cr-sk	between core and skin	
\dot{m}	mass flow rate	kg s^{-1}	dil	dilated	
m_{sw}	sweat rate	kg s^{-1}	fab	fabric	
P	vapor pressure	kPa	mrt	mean radiant temperature	
$P_{\text{sat, sk}}$	saturation vapor pressure at the skin temperature	kPa	perfusion, total	total blood perfusion	
Q_s	heat of adsorption	J kg^{-1}	r	radiative	
r	radius	m	sk, skin	skin	
R	local fabric regain	$(\text{kg of adsorbed H}_2\text{O kg}^{-1} \text{ fiber})$	s	sorptive	
R_d	combined air-clothing layer dry resistance	$\text{m}^2 \text{K W}^{-1}$	v	vein	
			<i>Greek subscripts</i>		
			∞	ambient	

(sweat generation), vasomotor response (control of skin blood flow rate) and for the fraction of total mass assigned to the skin layer. Gagge model is applicable for moderate activity levels and uniform environmental conditions [13], and is used to predict thermal comfort [14].

The first multi-segmented mathematical model of the entire human body was developed by Stolwijk [9,14]. His model uses five cylindrical segments to describe the human body: trunk, arms, hands, legs, feet, and a spherical head. Each segment is divided into four concentric lumped layers, representing core, muscle, fat and skin tissue layers. The segments are connected through blood flow in the arteries and veins offering an improved representation of the circulatory system and the distribution of heat within the body. Stolwijk's model of thermal control is described as functions of two tissue temperature signals as in Gagge's control system signals and the other is related to the rate of change of tissue temperatures [8,9]. The Stolwijk model does not recognize the flow in individual arteries and veins but uses a unique central blood node or pool at a uniform temperature. The constant temperature blood node exchanges heat with tissue layers by convection only, while tissue layers exchange heat in the segment by conduction only.

All subsequent contemporary multi-segment multi-mode bioheat models are modifications and improvements on Stolwijk model parameters and thermal control equations such as the Berkeley Comfort Model of Huizenga et al. [4], Tanabe and Kobayashi model [6], and Fiala et al. [15]. Several improvements were introduced in the Berkeley Comfort Model that include an increase in number of body segments, improved blood flow model for counter flow heat exchange in limbs, addition of a clothing node, and improved convection and radiation coefficients [4]. The Berkeley Model improved Stolwijk constant blood node temperature by using a thermoregulatory system that maintains the core temperature within a narrow range by either inhibiting or enhancing heat production and heat loss. The blood perfusion flow rates are based on Pennes' model [16].

The blood flow is a very important or decisive part of the human thermal functions. About 50–80% of the heat flow in the tissue is carried in or out of the tissue by the blood flow [16]. The Berkeley Comfort Model [4] improved some of Stolwijk model deficiencies but it did not use actual blood circulation network based on cardiac pulsating input that can predict exact core and skin blood flows. A detailed transient human body model known as the KSU Model was first developed by

Smith [13] using a three-dimensional finite element method and later improved by Fu [17] to include a clothing layer. They decompose the human body into fifteen cylindrical parts. KSU model allows having non-uniform and non-symmetric environmental conditions for each body element. The circulatory system is modeled with branching that initiates from the heart. The location of arteries and veins are the boundaries of each 3D finite element. The control equations for shivering, sudomotor and vasomotor are derived by Smith based on real experimental data. KSU model has a heavy computational time [13,17] and the blood system model parameters have been adjusted to fit experimental data using the blood perfusion flow in the capillary bed as input. Both Berkeley [4] and KSU [13] models ignore the effect of the pulsatile blood flow in the large arteries on heat transfer.

The clothing system plays a very important role in human thermal responses because it determines how much of the heat generated in the human body can be exchanged with the environment. The first clothing model was based on a simplified analytical solution of transient diffusion of heat and moisture transfer into textile materials [18]. Other thermal models of a piece of clothing that describe the moisture sorption in two stages were presented by David and Nordan [19]. Li and Holcombe [20] introduced another two-stage adsorption model to better describe the coupled heat and moisture transport in fabrics. Farnworth [21] developed a numerical model that takes into account the condensation and adsorption in a multi-layered clothing system. Jones [22] and Jones and Ogawa [23] developed another new unsteady-state thermal model for the whole clothing system. Li and Holcombe [20] presented their transient mathematical clothing model that describes the dynamic heat and moisture transport behavior of clothing and human body. Fu manipulated Jones and Ogawa model in order to model more than one layer of clothing worn by a human body. Fu model took into consideration the air layers between two consecutive clothing layers [17].

A multi-segmented passive human body model will be developed in this work to simulate the heat transfer within the body parts and the environment while combining the numerical simplicity of Stolwijk model [8,9] and using the most accurate and realistic representation of the arterial system including blood flow pulsation. The proposed model based on exact anatomical data of the human body will calculate the blood flow rates and their variations based on exact physiological data [1] to improve the heat exchange model. The circulatory system model will take into consideration the pulsatile blood flow in the arteries and the dependence of the arterial system on the heart rate and calculate the perfusion flow rates in the core. The model will be validated by comparisons with published experimental and simulation results on core and skin temperatures, and body latent heat loss when exposed to transient environment. A clothing mathematical model will be integrated to the transient nude human body model to simulate the thermal behavior of the human clothed body. The main objective for the integrated human-clothing model is to contribute to research efforts aimed at providing reliable predictions of human thermal responses over a wide range of environmental conditions.

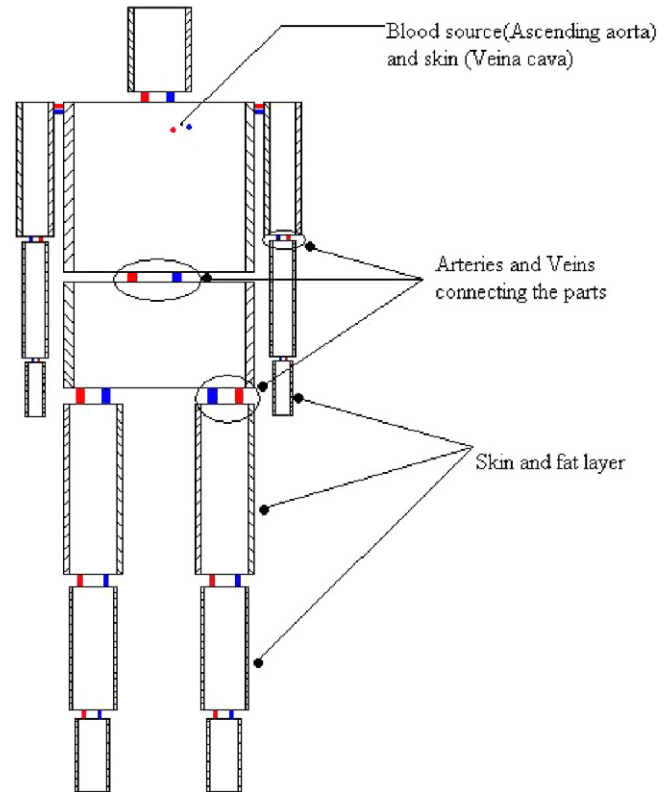


Fig. 1. Schematic of the multi-segment model.

2. Model description

The human body model divides the body into the fifteen body segment as shown in Fig. 1, where the trunk is divided into two segments, while the head and neck are combined in one segment. The other segments are the upper arms, thighs, forearms, calves, hands, and feet. Each segment is represented by a cylinder of a uniform temperature for each layer. The heat transfer model is based on four nodes: core, skin, artery and vein that exchange heat through convection, conduction and perfusion as shown in Fig. 2.

In any body segment, the blood exiting the arteries and flowing into the capillaries is divided into blood flowing in the core (exchanges heat by perfusion in the core) and blood flowing into the skin layer (exchanges heat by perfusion in the skin) after crossing the core tissue as shown in Fig. 2(a) [24–26]. The blood vessels (arteries and veins) contained in each segment of the body are identified [1,26–28]. Therefore, the blood entering a segment (from an artery) will split into a perfusion flow (including the skin blood flow) in the considered segment and a blood flow entering the adjacent segment. The opposite takes place in the veins for the same segment (see Fig. 2(b)). For peripheral segments (head, hand and foot), the blood entering rate is equal to the blood perfusion rate and the blood exiting rate. The heat generated by the human body is enhanced or dissipated to the environment through radiation, convection, and evaporation to maintain the core temperature within a narrow range.

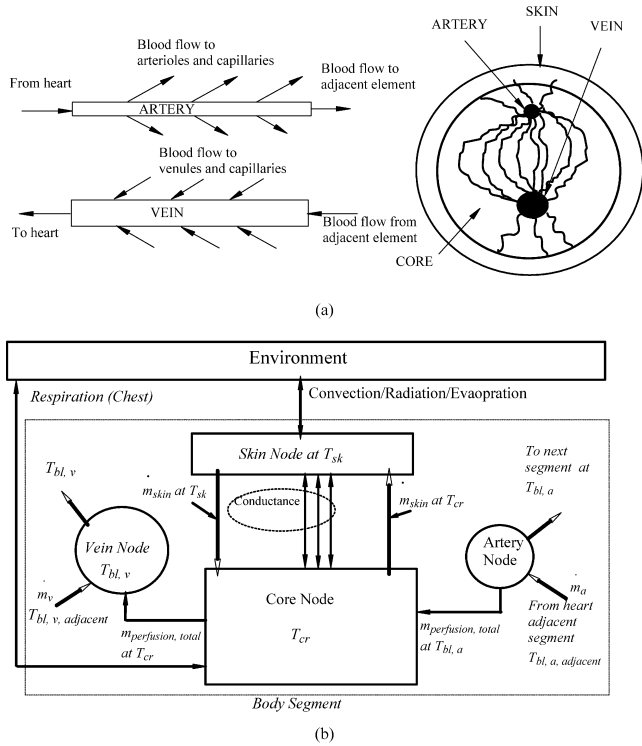


Fig. 2. A plot of the segment (a) blood flow in arteries and veins and (b) representation of core, skin, artery blood, and vein blood nodes and their interaction.

In the following section, a description will be give of the human circulatory system, and the unsteady bioheat equations for the core, skin, artery and vein nodes of each segment.

2.1. Human circulatory system

The blood vessels included in each segment are determined from geometrical, physiological and anatomical considerations [1]. The human circulatory system transports blood to all body tissues through an intrinsic network of blood vessels. In this work, the Avolio multi-branched model of the human arterial system is used where arteries are divided into 128 vessels starting from the central vessels to major peripheral arteries supplying the extremities including vessels of the order of 2.0 mm in diameter [1]. The arteries are represented by uniform thin-walled elastic tubes with realistic arterial dimensions and wall properties. The human circulatory system representation of the 128 vessels of the arteries is shown in Fig. 3 with lengths drawn proportional to actual vessel length while each artery vessel is identified by a branch number aj ($aj = 1$ to 128). The details of length and diameter of each cylindrical vessel can be found in Avolio’s work [1]. Table 1 lists for each body segment the associated arteries branch numbers and the segment inlet and exit artery vessel numbers that appeared in Fig. 3. The distribution of arteries and inlet and exit arteries in each body segment are given in Table 1. The blood vessels are assumed such that each artery–vein pair is represented by two parallel cylinders, as reported by Weinbaum and Jiji [27,28] with branches to peripheral skin layer to form the venules. The flow in veins (\dot{m}_v) is assumed non-pulsatile, and

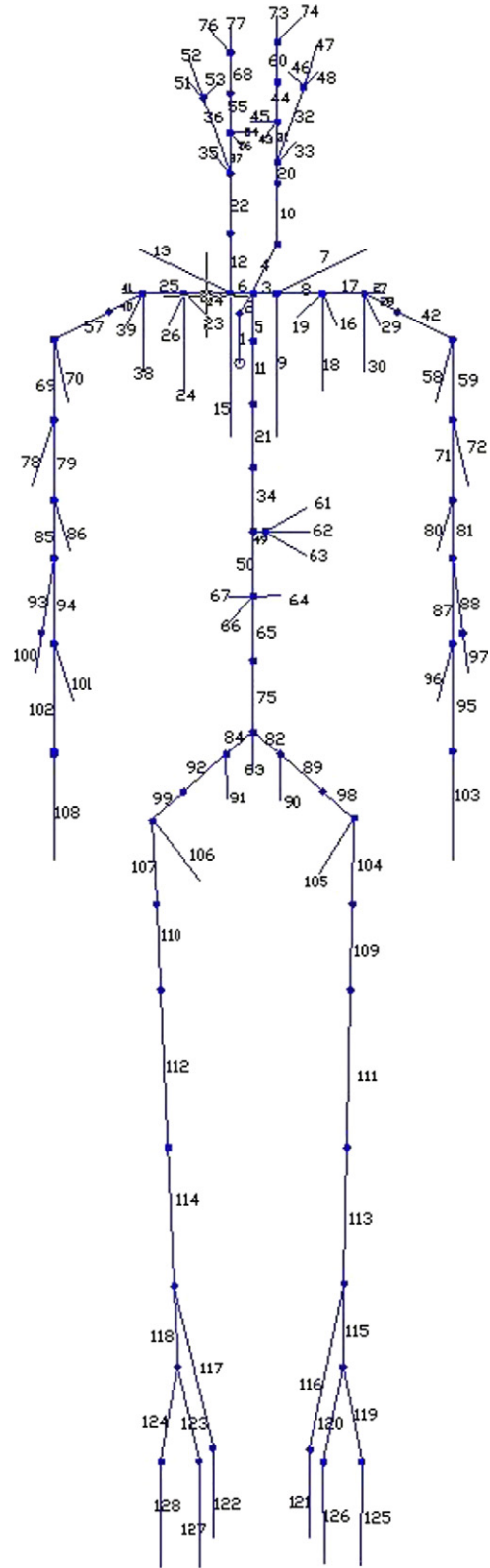


Fig. 3. The arteries model for blood flow calculations based on Avolio data [1].

is equal to the mean value of the corresponding artery flow (\dot{m}_a), [26,29]. Veins are bigger than arteries where the vein diameter is assumed equal to twice its corresponding artery diameter [13]. The inlet and outlet arteries/veins are assigned to

Table 1
Distribution of the arteries in each body part and inlet and outlet arteries of each segment [1]

Body element	The body segment associated arteries branch numbers <i>a_j</i> shown in Fig. 3							Inlet arteries vessel number	Outlet arteries vessel number
Head	22	10	20	33	31	32	46	4, 12	
	47	48	43	44	45	60	73		
	74	35	36	37	51	52	53		
	54	55	68	76	77				
Chest	4	12	13	7	3	6	2	1	42, 57, 4, 12, 34
	5	8	16	17	18	19	27		
	28	29	30	14	23	24	25		
	26	40	38	39	11	21	34		
	9	15							
Pelvis	49	61	62	63	50	64	65	34	89, 92
	66	67	75	82	83	84	91		
	92	99	90	89	98				
Left upper arm	57	69	70	78	79	85	86	42	81
Left fore arm	93	100	94	101	102			81	103
Left hand	108							103	
Left thigh	106	107	110	112				89	113
Left calf	114	117	122	118	123	124		113	125
Left foot	127	128						125	
Right upper arm	42	58	59	71	72	80	82	57	85
Right fore arm	88	97	87	95	96			85	108
Right hand	103							108	
Right thigh	104	105	109	111				92	114
Right calf	113	116	121	115	119	120		114	127
Right foot	125	126						127	

each of the fifteen body segment. The Avolio’s multi-branched human arterial system network of pulsatile flow initiates from the heart and branches throughout the body [1]. The cardiac output and the heart rate are correlated to the total metabolic rate [30].

The heart rate and the physical, geometrical and elastic properties of the arteries are the inputs to Avolio model. Avolio model predicts characteristic impedance, propagation constant, wave reflection coefficient, and input impedance for each artery. The velocity ratio is calculated between any two adjacent arteries in Avolio’s arterial tree starting from the peripheral arteries towards the ascending aorta [1]. If the velocity is known at the ascending aorta from the heart, then velocities in all arterial tree are determined. The contribution of the veins system is taken into consideration as boundary condition on the peripheral arteries. The cardiac ejection waveform which is the temporal blood velocity variation in the ascending aorta is available in literature for the basal heart rate of 75 beats per minute where the basal cardiac output is 290 006 cm³ hr⁻¹ [31]. This periodic function is treated by Fourier series [26,29,32] and multiplied by the complex velocity ratios found by Avolio model to derive the blood velocity in each artery at that heart rate and cardiac

output. To determine the ejection waveform at other metabolic rates, the stroke volume is almost constant since it is related to the anatomical heart size [33]. The change in the cardiac output due to exercise or shivering is calculated using the following equation [17]:

$$CO = \frac{M_{total}}{M_{basal}} \cdot \frac{CO_{dil} \cdot CO_{con}}{CO_{basal}} \quad (1)$$

where M_{total} is the total metabolic rate, M_{basal} is the thermoneutrality metabolic rate, CO_{basal} is the cardiac output at thermoneutrality condition, CO_{con} is the constricted cardiac output and CO_{dil} is the dilated cardiac output defined in Fu thermoregulatory control equations for cardiac output [17]. The actual cardiac output Eq. (1) is restricted by the upper and lower limits of the cardiac outputs of $CO_{max} = 427\,500 \text{ cm}^3 \text{ hr}^{-1}$ and $CO_{min} = 270\,000 \text{ cm}^3 \text{ hr}^{-1}$. The excess metabolic rate due to exercise causes a significant increase in the heart rate, the heart rate in beats/minute is found in terms of the total metabolic rate M_{total} (W) using the following correlation of ASHRAE [30]:

$$\text{Heart rate} = 3.4(0.0476M_{total} - 7) + 75 \quad (2)$$

The new wave form is determined by adjusting the amplitude by the ratio of the new cardiac output to the basal cardiac out-

put and adjusting the period to the new heart rate. The velocity amplitude in the ascending aorta is then calculated for new heart rate different than the 75 beats/min at thermal neutrality.

The computed artery and vein blood flow rates (\dot{m}_a, \dot{m}_v) are used for evaluating the corresponding heat transfer coefficients in the arteries and veins, respectively. The convective heat transfer coefficient of pulsating flow ($h(t)$) in main arteries is used in the model [34,35]. Pulsating flow in main arteries induces 6–10% increase of the average unsteady heat transfer coefficient from steady-state value while for arterioles the difference between unsteady and steady heat transfer is insignificant and is independent of the pulsation frequency [34]. For a large amplitude pulsation in laminar pipe flow, the heat transfer due to pulsation is always augmented [35].

The perfusion blood flow rate ($\dot{m}_{\text{perfusion}}$) through the capillaries is calculated by subtracting the exiting flow from the entering blood flow of the considered segment. Larger arteries, veins, and arterioles are assumed to exchange heat by convection with the core of the body. The venules located in the tissue (skin and core) exchange heat between the core and the skin. These small vessels play a major role in thermoregulation where the skin blood flow varies as a function of the core and skin temperatures [13]. The circulatory system model is used to predict the blood flow in the arteries and veins and perfusion rates in the core while the skin perfusion blood flow is calculated based on empirical and experimental correlations reported by Fu [17]. The information is then used to update the energy balances of each body segment.

2.2. Energy balance equations

For each segment, the heat balance equation is written for each of the four nodes (core, skin, artery blood, and vein blood) [9] shown in Fig. 2.

2.3. Core and skin nodes energy balances

The core node energy balance is given by

$$\begin{aligned}
 C_{\text{cr}} \cdot \frac{dT_{\text{cr}}}{dt} &= M_{\text{cr}} + M_{\text{shiv}} - W - \alpha \cdot Q_{\text{res}} - Q_{\text{cr-sk}} \\
 &- \underbrace{\left[\sum_{\substack{\text{arteries} \\ \text{arterioles}}} h(t) \cdot A_{\text{artery}} \right] \cdot [T_{\text{cr}} - T_{\text{bl},a}]}_{\text{Arteries heat exchange by convection}} \\
 &- \underbrace{\left[\sum_{\text{veins}} h_{\text{mean}} \cdot A_{\text{vein}} \right] \cdot [T_{\text{cr}} - T_{\text{bl},v}]}_{\text{Veins heat exchange by convection}} \\
 &+ \underbrace{\dot{m}_{\text{perfusion,total}} \cdot c_{\text{bl}} \cdot (T_{\text{bl},a} - T_{\text{cr}})}_{\text{Core perfusion heat exchange}} \\
 &+ \underbrace{\dot{m}_{\text{skin}} \cdot c_{\text{bl}} \cdot (T_{\text{sk}} - T_{\text{cr}})}_{\text{Skin perfusion heat exchange}} \quad (3)
 \end{aligned}$$

where C_{cr} is the thermal capacitance of the segment core, α is equal to unity for the chest and zero for all other elements, W is

the mechanical work generated by the body, Q_{res} is the heat dissipated by respiration calculated based on the known ASHRAE correlations [30], $h(t)$ is the pulsating heat convection coefficient of the blood flow, h_{mean} is the mean non-pulsating convection coefficient of blood flow in veins, $\dot{m}_{\text{perfusion,total}}$ is the total perfusion rate of blood entering the core; \dot{m}_{skin} is the skin perfusion blood flow, A_{artery} or A_{vein} is the surface area of the blood vessel, M_{cr} is the basal metabolic heat generated in each segment [13], and M_{shiv} is the segmental thermoregulatory metabolic rate generated by shivering. The respiration heat loss by convection and evaporation is considered to be associated to the chest where most of the dissipation occurs [6,13]. The heat dissipation by respiration in the head segment is negligible compared to the total heat dissipation of the head. Bioheat models of Smith [13] and Tanabe et al. [6] used the same assumption. The blood specific heat c_{bl} is taken as $4000 \text{ J kg}^{-1} \text{ K}^{-1}$. The term on the left-hand side of Eq. (3) is the rate of accumulation of thermal energy per unit volume due to the changing temperature of core tissue. The last four terms on the right-hand side of Eq. (3) represent: the heat exchange between the core node and the arteries by convection, the heat exchange with veins by convection; the net heat flow associated with perfusion blood flow through capillaries entering the core at the arteries blood temperature and leaving at the core temperature [10,24,30]; and the net heat exchange associated with perfusion blood flow, \dot{m}_{skin} , between the skin and the core node. The heat transfer coefficient $h(t)$ is obtained from isothermal wall correlation at $T_{\text{bl},a}$ and using the instantaneous pulsating velocities obtained from the human circulatory model. The summation of the product of the arteries and arterioles surface areas with their corresponding pulsating heat transfer coefficients ($\sum_{\text{arteries and arterioles}} h(t) \cdot A_{\text{artery}}$) is performed over all the artery branches in the segment under consideration. Similarly, the summation of the product of the veins and venules surface areas with their corresponding mean convection coefficient is done for all the veins and venules of the segment under consideration. The heat exchanged between the skin and the core through the contact thermal resistance is $Q_{\text{cr-sk}}$ and is given by

$$Q_{\text{cr-sk}} = K \cdot (T_{\text{cr}} - T_{\text{sk}}) \quad (4)$$

where K is the skin to core conductance. The values of K are based on the correlations of Havenith [36] and the physiological data of Gordon [31]. The core and the skin temperatures depend strongly on the change of the perfusion blood flow rate through the muscle as calculated from the circulatory system model based on the cardiac output and the heart rate. The model formulation assumes complete thermal equilibrium between blood and tissue [17,24] for all body parts meaning that the blood exiting the core node and entering the vein node is at core temperature. The thermal equilibrium assumption proves its validity because the blood flow through the core tissue is very slow [2]. Another argument that supports this assumption is that the core and blood system can be assimilated to heat exchanger with a very high heat transfer area, area/volume ≈ 5000 as calculated from Milnor's data [26]. This large heat transfer

area makes the outlet blood temperature equal to the core temperature.

The skin node energy balance is given by

$$C_{sk} \cdot \frac{dT_{sk}}{dt} = M_{sk} + Q_{cr-sk} - A_{sk} \cdot [h_c \cdot (T_{sk} - T_{\infty}) + h_r \cdot (T_{sk} - T_{mrt}) + h_e \cdot (P_{sk} - P_{\infty})] + \underbrace{\dot{m}_{skin} \cdot c_{bl} \cdot (T_{cr} - T_{sk})}_{\text{heat transfer through the skin blood flow}} \quad (5a)$$

where C_{sk} is the thermal capacitance of the segment skin node, h_c is the external convection heat transfer coefficient between the skin and the atmosphere, h_r is the radiation transfer coefficient, h_e is the evaporation coefficient deducted from h_c by Lewis formula [23], T_{∞} is the surroundings radiant temperature, P_{∞} is the ambient vapor pressure, and P_{sk} is the skin vapor pressure as expressed by Jones [21]

$$P_{sk} = \frac{P_{sat,sk} \cdot I_{a-sk} + P_a \cdot I_{sk} + m_{sw} \cdot h_{fg} \cdot I_{sk} \cdot I_{a-sk}}{I_{sk} + I_{a-sk}} \quad (5b)$$

where I_{sk} is the evaporative resistance of the skin which is approximately $0.33 \text{ m}^2 \text{ kPa W}^{-1}$ for a well hydrated person, I_{a-sk} is the evaporative resistance of the adjacent air layer in $\text{m}^2 \text{ kPa W}^{-1}$ and m_{sw} is the local sweat rate ($\text{kg m}^{-2} \text{ s}^{-1}$) [17]. The value of the skin vapor pressure is subject to the constraint that the vapor pressure calculated in Eq. (5b) cannot exceed the saturation pressure at T_{sk} . Eq. (5b) applies even if the sweat rate is zero. Jones [22] included in the boundary condition the accumulation of moisture on the skin and the evaporation of that moisture through a mass balance at the skin surface subject to the constraint that the accumulated moisture is less than 0.035 kg m^{-2} based on the maximum sweat layer that can be sustained over the body which is about $35 \mu\text{m}$ [22].

2.4. Arteries and veins blood nodes energy balance

The arteries node energy balance is given by

$$C_{bl,a} \cdot \frac{dT_{bl,a}}{dt} = - \left[\sum_{\substack{\text{arteries} \\ \text{arterioles}}} h(t) \cdot A_{\text{artery}} \right] \cdot [T_{bl,a} - T_{cr}] + \dot{m}_a \cdot c_{bl} \cdot (T_{bl,a,adjacent} - T_{bl,a}) \quad (6)$$

where \dot{m}_a is the mass flow rate of blood entering the considered part through the inlet artery, and \dot{m}_a is assumed to change with time within one period of pulsation like the cardiac ejection waveform. Note that for the chest, there is no adjacent element, but the blood enters the chest from the heart at the same rate of blood returning from the veins through the vena cava.

The vein node energy balance is given by

$$C_{bl,v} \cdot \frac{dT_{bl,v}}{dt} = - \left[\sum_{\text{veins}} h_{\text{mean}} \cdot A_{\text{vein}} \right] \cdot [T_{bl,v} - T_{cr}] + \dot{m}_v \cdot c_{bl} \cdot (T_{bl,v,adjacent} - T_{bl,v}) + \dot{m}_{\text{perfusion,total}} \cdot c_{bl} \cdot (T_{cr} - T_{bl,v}) \quad (7)$$

where \dot{m}_v is the mass flow rate of blood entering the considered part through the inlet vein and $\dot{m}_{\text{perfusion,total}}$ is the perfusion blood flow rate in the considered part where it enters the venous bed at core temperature and leaves at vein temperature.

2.5. Thermoregulatory control equations

The thermal signals affect the quantity of blood flowing in the muscles tissue by increasing or decreasing the amplitude of the pulsating cardiac output and the skin blood flow by the mechanisms of vasodilation and vasoconstriction that result in a higher or lower skin blood flow, respectively. The correlations depend on the mean skin temperature and on the head core temperature. If the vasodilation thermoregulatory function is not sufficient to reject the heat from the body, the sudomotor function is triggered where heat is lost by sweating [13,17]. On the other hand, if vasoconstriction is not able to keep the heat in the body, metabolic thermoregulatory function takes place; the body will start shivering in order to heat the body. The sudomotor and metabolic thermoregulatory functions follow the KSU model of Smith [13] and Fu [17] and will not be presented here. For vasomotor, the skin perfusion blood flow rate is evaluated from the thermal control equations which determine the thermal interaction between the skin and core by blood perfusion. The vasomotor control equations are formulated based on basal skin blood flow rate $\dot{m}_{\text{skin,basal}}$, maximum skin blood flow rate $\dot{m}_{\text{skin,max}}$, and minimum skin blood flow rate $\dot{m}_{\text{skin,min}}$ (see Table 2) as follows:

$$\dot{m}_{\text{skin}} = \frac{\dot{m}_{\text{skin,dil}} \cdot \dot{m}_{\text{skin,con}}}{\dot{m}_{\text{skin,basal}}} \quad (8a)$$

$$\dot{m}_{\text{skin,dil}} = \begin{cases} \dot{m}_{\text{skin,basal}} & \text{for } T_{cr} \leq 36.8^\circ\text{C} \\ \frac{T_{cr}-36.8}{37.2-36.8} \cdot (\dot{m}_{\text{skin,max}} - \dot{m}_{\text{skin,basal}}) + \dot{m}_{\text{skin,basal}} & \text{for } 36.8^\circ\text{C} < T_{cr} < 37.2^\circ\text{C} \\ \dot{m}_{\text{skin,max}} & \text{for } T_{cr} \geq 37.2^\circ\text{C} \end{cases} \quad (8b)$$

$$\dot{m}_{\text{skin,con}} = \begin{cases} \dot{m}_{\text{skin,min}} & \text{for } T_{sk} \leq 27.8^\circ\text{C} \\ \frac{T_{sk}-27.8}{33.7-27.8} \cdot (\dot{m}_{\text{skin,basal}} - \dot{m}_{\text{skin,min}}) + \dot{m}_{\text{skin,min}} & \text{for } 27.8^\circ\text{C} < T_{sk} < 33.7^\circ\text{C} \\ \dot{m}_{\text{skin,basal}} & \text{for } T_{sk} \geq 33.7^\circ\text{C} \end{cases} \quad (8c)$$

Values of $\dot{m}_{\text{skin,basal}}$, $\dot{m}_{\text{skin,max}}$, and $\dot{m}_{\text{skin,min}}$ are given in Table 2 [17].

2.6. Integration of clothing model

The transient mathematical model for a layer of clothing element is developed based on Jones model [37] neglecting the effect of moisture in the fabric interstices. Each fabric layer is assimilated to a cylinder that is suitable to the shape of the body segments and the heat and mass flows are assumed to take place only in the radial direction. The evaporative and dry resistances of the fabrics are assumed constant. The mass and heat diffusion in a clothing layer can be formulated by the following equations, respectively, written in the radial direction as presented by Jones [37]:

$$\rho_{\text{fab}} \frac{\partial R}{\partial t} = \frac{e_{\text{fab}}}{R_{e,\text{fab}} \cdot L} \left(\frac{1}{r} \frac{\partial P}{\partial r} + \frac{\partial^2 P}{\partial r^2} \right) \quad (9a)$$

Table 2
Basic body parameters used in the model at basal metabolic generation [1,13,17,30,31]

Body segment	Skin area (m ²)	Length of the body cylindrical segment (m)	Basal core metabolic rate (W)	Basal skin metabolic rate (W)	Core thermal capacitance [C _{cr}] (JK ⁻¹)	Core thermal capacitance [C _{cr}] (JK ⁻¹)	Skin conductance (W K ⁻¹)	Artery ^a blood thermal capacitance (JK ⁻¹)	Vein ^a blood thermal capacitance (JK ⁻¹)	Basal skin blood flow at thermoneutrality (cm ³ hr ⁻¹)	Min. skin blood flow at maximum vasoconstriction (cm ³ hr ⁻¹)	Max. skin blood flow at maximum vasodilation (cm ³ hr ⁻¹)	Skin thickness (mm)
	[13,17]	[13]	[17,30]	[17,30]	[13,17]	[13,17]	[31,36]	[1,13,17]	[1,13,17]	[17]	[17]	[17]	[31]
Head	0.1414	0.384	18.433	0.218971	12.247.09	1710.151	1.8476	810.478	2.482.089	6050	4518	16552	8.5
Chest	0.4021	0.4925	5.95	0.6	36.732.08	13624.81	4.9212	2.266.76	6941.953	3.441.5	0	33.246	19.12
Pelvis	0.2465	0.324	46.86	0.6	67.160.54	13624.81	4.9212	566.69	1735.488	2.272.5	0	21.953	19.12
Upper arm	0.0998	0.353	1.0619	0.181965	6.707.916	1.284.016	1.304	49.596	151.8878	910	0	8.319	4.51
Fore arm	0.0679	0.292	0.593	0.100896	3.750.124	717.863	0.913	32.355	99.08719	508	0	5.553	4.51
Hand	0.045	0.30	0.095	0.093	791.358	723.468	0.5452	21.441	65.66306	1.114	627	4.454	7.4
Thigh	0.1482	0.352	1.708	0.342824	11.926.27	4.133.92	1.5637	93.083	285.0667	1.456	0	12.453	10.64
Calf	0.1024	0.379	0.754	0.152983	5.262.342	1.850.759	1.216	36.755	112.5622	651	0	8.253	10.64
Foot	0.0586	0.241	0.146	0.12699	1.465.253	1.347.373	0.6311	18.687	57.22894	934	301	5.278	11.7

^a The value of the capacitance is based on the mass of blood present in artery or vein in the body segment at basal conditions.

$$c_{fab} \rho_{fab} \frac{\partial T}{\partial t} = \frac{e_{fab}}{R_{d, fab}} \left(\frac{1}{r} \frac{\partial T}{\partial r} + \frac{\partial^2 T}{\partial r^2} \right) + \rho_{fab} Q_s \frac{\partial R}{\partial t} \quad (9b)$$

where R is the local regain, P is the vapor pressure in the clothing layer, ρ_{fab} is the fabric density, c_{fab} is the fabric specific heat, e_{fab} is the fabric thickness, $R_{e, fab}$ and $R_{d, fab}$ are the fabric evaporative resistance and dry resistance, respectively, L is the water heat of vaporization, and Q_s heat of adsorption. The local relative humidity in each clothing layer is related to the regain through empirical curves depending on fiber material [38]. The physical nature of the clothing system allows simplification of the model. Multiple clothing layers are separated by air layers that have a very small adsorptive and thermal capacitances compared to the clothing layers [37]. The thermal transient effect of the air layers can be neglected. However, air has low thermal conductivity and small thickness allows a lumped approximation of temperature and regain in the air layer. For thin clothing layers, each layer can be lumped with its corresponding air layer to form a clothing node. In the differential equations (9a) and (9b), the evaporative and dry resistances will be replaced by the combined air-clothing layer evaporative resistance $R_e (= R_{e, fab} + R_{e, air})$ and dry resistance $R_d (= R_{d, fab} + R_{d, air})$, respectively [37]. The radial diffusion terms of vapor and heat can then be based on the driving vapor pressure and temperature differences over each combined layer.

3. Numerical method

A simulation program was developed. The input to the program consisted of the initial thermal state of the human body, the metabolic rate, the ambient conditions, and the physiological and physical parameters inherent in the bioheat model of the human body. Table 2 lists all the relevant human body physical and thermal parameters used in the simulation model and their references. A fully explicit first order Euler–Forward integration scheme with a time step Δt of 0.02 s over the desired simulation period was used to solve the energy balance equations of the human body nodes for any segment where the respiratory heat loss, blood flow rates, thermoregulatory responses and skin vapor pressure were calculated from previous time step. The regional blood flow rates in the arteries, veins, and tissue were obtained from the output of Avolio model which consists of the velocity ratios for any considered artery to the cardiac output. Therefore, the temperatures of the core, skin, artery, and vein nodes, and the artery blood flow rate are updated for each segment at each time step. Avolio model blood flow that gives the arterial blood velocity and the blood perfusion rates was computed after each complete cycle of the heart which approximately takes 0.8 s for the neutral state of the body and can vary depending on the metabolic rate. Numerical tests were for uniform time step sizes of 0.02 s, 0.01 s, and 0.005 s. The time step of 0.02 s was found to be of sufficient accuracy at relative error of less than 0.008% in values of blood flow rates compared to the lower time step and 10–4% in temperature. In transient simulations, a smaller time step size of 0.001 s was used at the times when sudden change in environment temperature or metabolic rate takes place. In transient simulations, suitable initial conditions were determined starting from the neutral conditions of

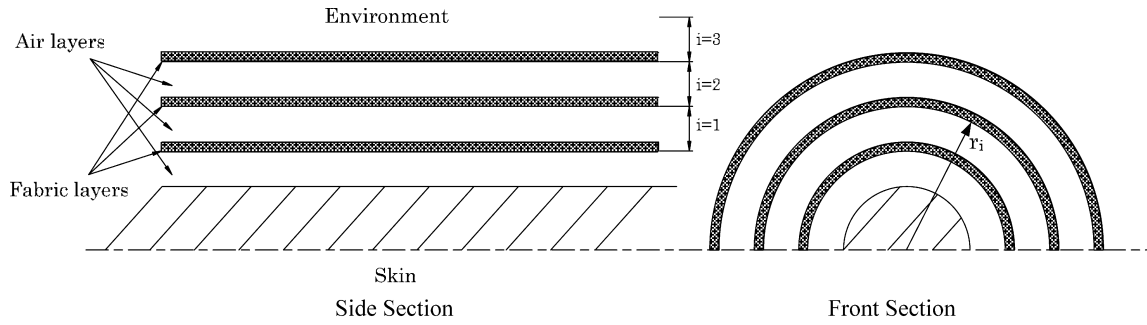


Fig. 4. Schematic of the multi-layer clothed body element.

$T_{cr} = 36.8^{\circ}\text{C}$, and $T_{sk} = 33.7^{\circ}\text{C}$ to simulate a relatively long exposure to any pre-conditioning environment. The obtained steady state values were then used as initial conditions for all other unsteady calculations of various node temperatures for all segments and the sensible and latent heat loss from the skin.

The clothing equations are discretized using an explicit Euler–Forward first order integration scheme. However, because of the multiple clothing layers on each body segment, spatial discretization is needed in the radial direction for both the clothing and air layers. Fig. 4 shows the fabric and air layers. The mass and energy balances of a clothing-adjacent-air-layer of Eq. (9) reduces to the following:

$$e_{fab,i} \cdot \rho_{fab,i} \cdot L \cdot \frac{\Delta R_i}{\Delta t} = \frac{r_{i-1}}{r_i} \cdot \frac{P_{i-1} - P_i}{R_{e,i-1}} - \frac{P_i - P_{i+1}}{R_{e,i}} \quad (10a)$$

$$e_{fab,i} \cdot c_{fab,i} \cdot \rho_{fab,i} \cdot \frac{\Delta T_i}{\Delta t} = \frac{r_{i-1}}{r_i} \frac{T_{i-1} - T_i}{R_{d,i-1}} - \frac{T_i - T_{i+1}}{R_{d,i}} + e_{fab,i} \cdot \rho_{fab,i} \cdot Q_{s,i} \frac{\Delta R_i}{\Delta t} \quad (10b)$$

where i is the index of the clothing layer. The coupling of the solution of the clothing system to the nude body model occurs at the skin where the skin node energy balance equation (3) is modified for the clothed element to represent skin heat losses to the adjacent air layer rather than the environment.

4. Results and discussion

4.1. Arterial circulation

The arterial circulation system is validated against published experimental data of Mills et al. [39] and simulation model of Avolio [1] by comparing the input impedance frequency response at the ascending aorta to the applied cardiac ejection waveform. Fig. 5 shows (a) the input impedance amplitude and (b) the input impedance phase as function of the pulsation frequency for the current model and the published data. The current work simulation results agree well with the experimental data and the model of Avolio for the impedance amplitude vs. frequency has better agreement with experimental data on impedance phase at high frequencies. The better results of our

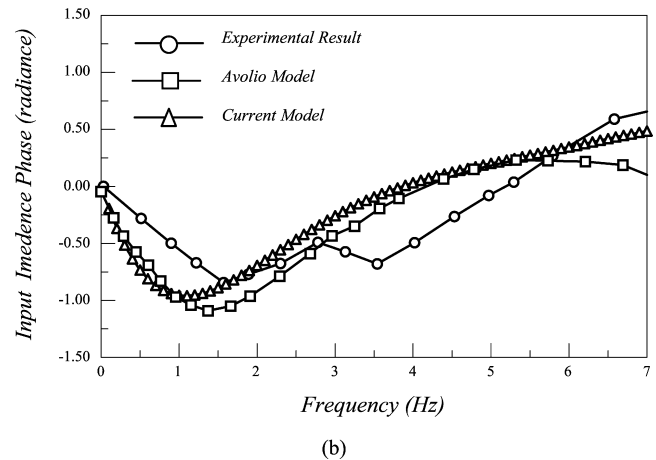
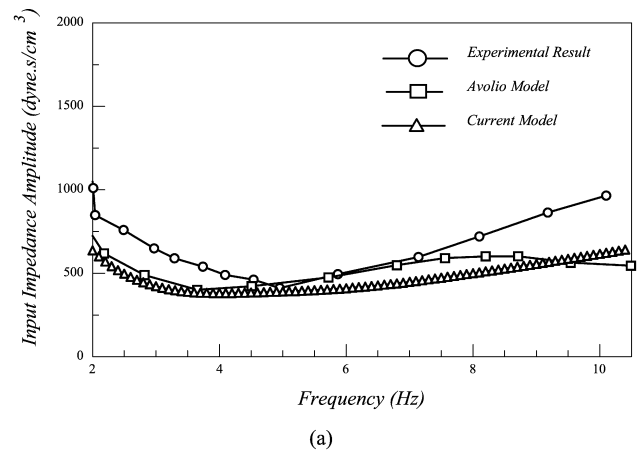


Fig. 5. A plot of (a) the input impedance amplitude and (b) the input impedance phase as function of the pulsation frequency for the current model and the published data [1].

model stem from the treatment of the Bessel functions where they are calculated on analytical expressions and not from the use of empirical formulae for the tabulated values in Womersley solution [2]. The program is run at smaller frequency steps of 0.05 compared to 0.5 of Avolio model. The arterial system is used to calculate blood flow rate to each body segment and the amount of blood perfusion rates that carried from the core to the skin node. Table 3 presents the basal perfusion blood flow rate calculated using the current model and the published experimental perfusion flow rates of Gordon [31] and Ganong [40]. The circulatory model simulation results show good agreement

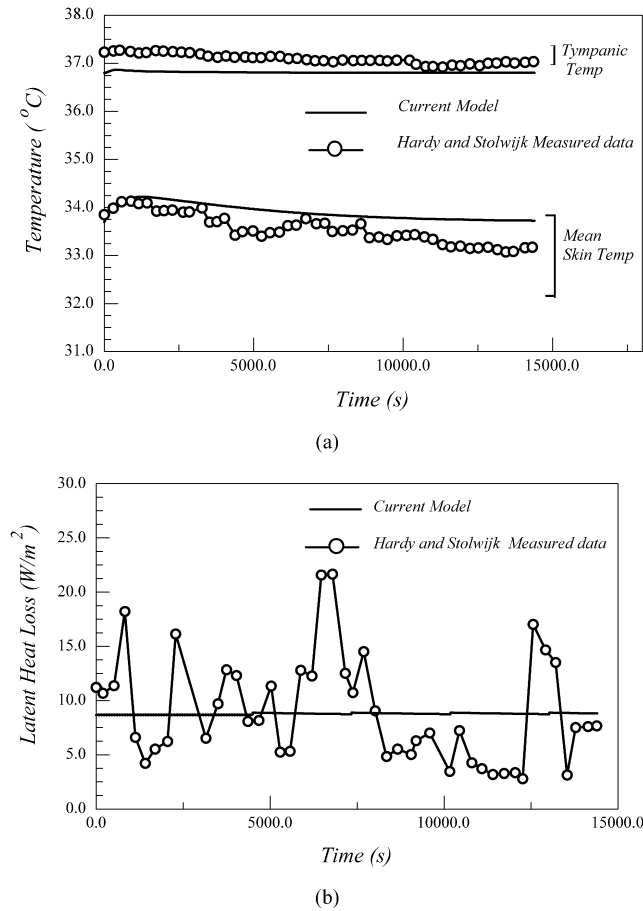


Fig. 6. The measured data of Hardy and Stolwijk [41] and simulated results of (a) tympanic and mean skin temperature, and (b) latent heat loss as a function of time at $T_{\infty} = 28.5^{\circ}\text{C}$ and $RH_{\infty} = 31\%$.

Table 3
Calculated basal perfusion blood flow rate $\dot{m}_{\text{perfusion, (basal)}}$ of the current model and the published experimental data of Gordon [31] and Ganong [40]

Segment	Calculated perfusion flow rate from current model ($\text{cm}^3 \text{hr}^{-1}$)	Experimental perfusion flow rate [31,40] ($\text{cm}^3 \text{hr}^{-1}$)	Relative error (%)
Head	58 829	56 526	4.1
Chest	194 352	198 164	1.9
Upper arm	3 577	3 852	7.1
Fore arm	2 266	2 152	5.3
Hand	1 502	1 378	9.0
Thigh	6 520	6 196	5.2
Calf	2 531	2 741	7.7
Foot	1 288	1 339	3.8
Total cardiac output	288 549	290 006	0.5

with published data where the error is as low as 1.9% in the chest and is highest in the hand at 9%.

4.2. Nude body model validation

The multi-segmented model is validated by comparing simulated skin, tympanic and rectal temperatures with published experimental and simulation data of other models for a vari-

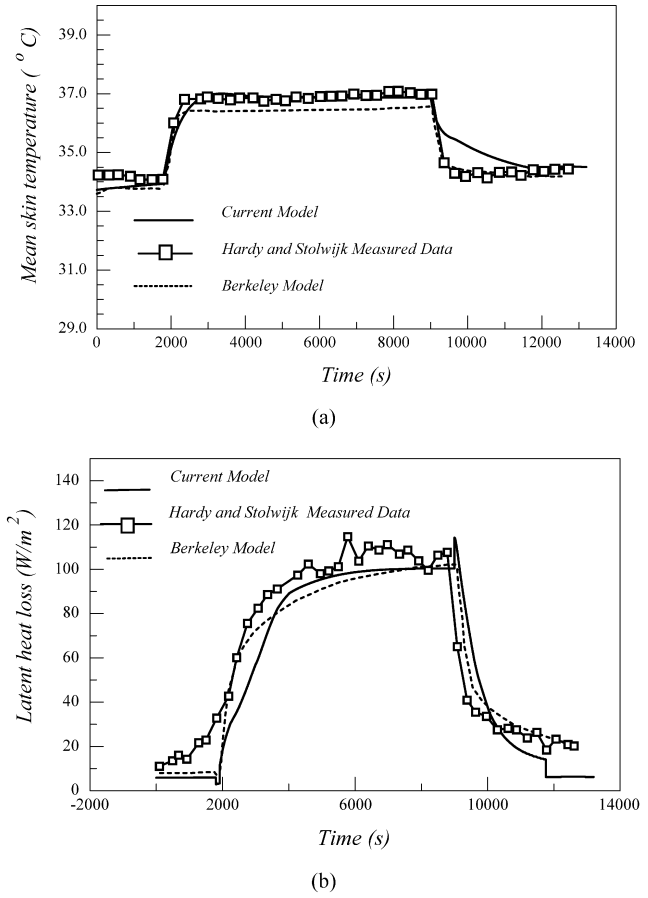
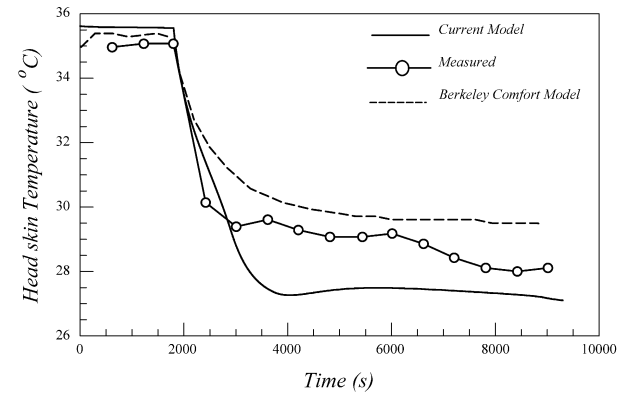


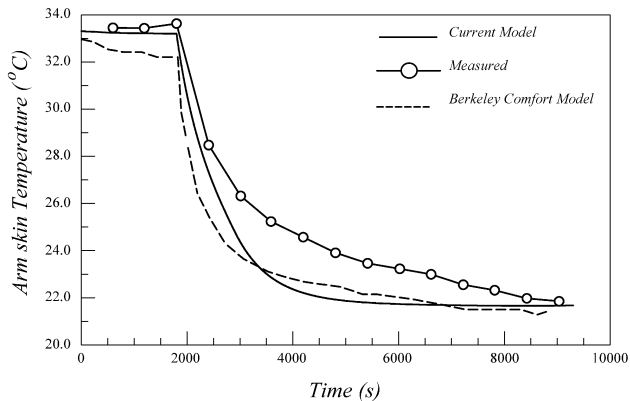
Fig. 7. The measured data of Hardy and Stolwijk [41] and predicted (a) mean skin temperature and (b) evaporative heat loss in addition to the results of the Berkeley Comfort Model [4].

ety of ambient and activity levels in steady-state and transient conditions. In addition to experimental comparison, simulation results will be compared with results of a computationally detailed model predictions of Smith [13], and to the recent improved predictions of the Berkeley Model. For a sedentary human condition, Hardy and Stolwijk reported experimental data of the mean skin temperature for resting human subjects who wore only shorts [41] for an exposure period of four hours to ambient temperature of $T_{\infty} = 28.5^{\circ}\text{C}$ and relative humidity $RH_{\infty} = 31\%$ at metabolic rate $M = 1$ met at neutrality. Fig. 6 presents the simulated results of current model of (a) tympanic and mean skin temperature, and (b) latent heat loss as a function of time in addition to the reported experimental data of Hardy and Stolwijk [41] at the same conditions. Under steady-state conditions, the mean skin and tympanic temperature predictions are very close to the measured values within 0.5°C . The latent heat loss agrees well with experimental measurement.

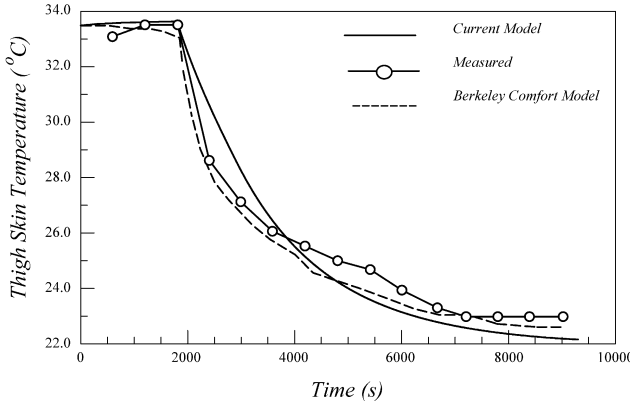
The second comparison with measured data and models is for a hot-exposure transient of Hardy and Stolwijk [41]. The reported experimental data were done for a step change in environment temperature from 30°C at 40% RH to 48°C at 30% RH for an exposure period of two hours followed by one hour of environment at 30°C at 40% RH. Fig. 7 shows the measured [41] and predicted (a) mean skin temperature and (b) evaporative heat loss in addition to the results of the



(a)



(b)

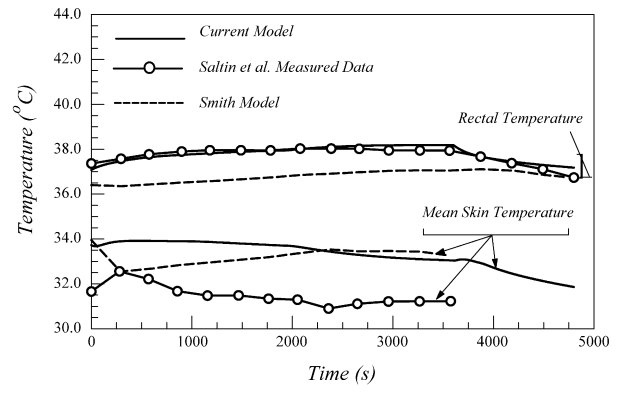


(c)

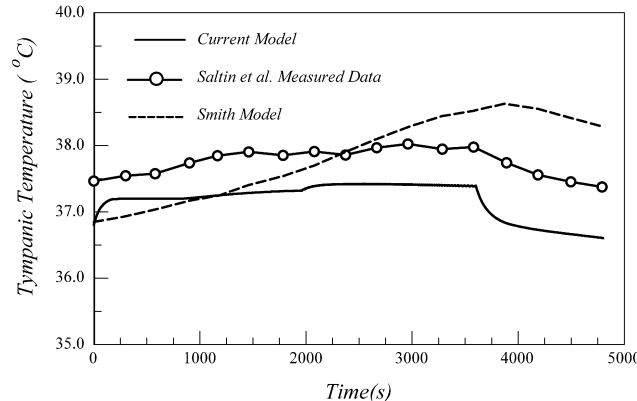
Fig. 8. The measured data of Raven and Horvath [42] and simulated temperatures of current model and Berkeley model [4] for a step change from 28 to 4.7 °C for (a) head skin temperature; (b) upper arm; and (c) thigh.

recent Berkeley Comfort Model [4]. During the hot interval the current model predicted well the mean skin temperature and latent heat loss, and produced comparatively similar results to Berkeley Model predictions. The core-skin convection interaction is well represented in the current model due to the use of a more realistic circulatory blood flow system for the macro and micro circulation effect on convection heat exchange.

The third comparison with measured data and models is for a cold-exposure transient of Raven and Horvath [42] from



(a)



(b)

Fig. 9. The measured data of Saltin et al. [43] and predicted values of current model and Smith Model [13] of (a) rectal and mean skin temperature; and (b) tympanic temperature; and (c) mean skin temperature in constant environment of 20.5 °C, 55% RH for a step change in metabolic rate.

a cold step change in ambient temperature from 28.5 °C, 45% RH to 4.7 °C, 70% RH for a period of two and a half hours. Fig. 8 shows the measured [35] and simulated temperatures for a step change from 28 to 4.7 °C for (a) head skin temperature; (b) upper arm; and (c) thigh. The blood flow model has shown good agreement with experimental data in limbs and extremities skin temperature predictions comparable to the agreement shown in the Berkeley Model [4].

Another comparison for the nude body model is performed against measured data of Saltin [43] at constant environment temperature 20.5 °C, 55% RH with a step change in metabolic rate from $M = 4.14$ met continuing for a period of 60 minutes followed by a 20 minute rest period at $M = 1$ met. Fig. 9 shows the measured [43] and predicted values of current model of (a) rectal and mean skin temperatures and (b) tympanic temperature in constant environment of 20.5 °C, 55% RH for a step change in metabolic rate. On the same plot Smith Model published simulation data [13] are shown. The rectal and tympanic temperatures agreed rather well with experimental results and have shown comparable level of agreement with Smith 3-D model results with deviations from experimental data of less than 0.5 °C. However, the predicted mean skin temperature of current model and that of Smith ran two degrees higher than experimental values of Saltin [43]. The agreement with the mean

skin temperature at a high sweat rate may not be critical since the reported experimental data have indicated an environmental chamber temperature between 19 and 22 °C and relative humidity between 45–65%, while the simulations are done at the mean fixed ambient condition of 20.5 °C and the mean relative humidity at 55%.

4.3. Clothed model validation

The clothed model validation is performed by the results comparison against measured data of Jones and Ogawa [23] at constant environment relative humidity of 50%, constant activity level of $M = 1$ met and constant temperature of 21.1 °C (70 F) continuing for a period of 3600 s (60 minutes). The test was preceded by 2700 s (45 minutes) exposure to a cold environment of 4.4 °C (40 F). The fabric composition and the fabric physical and thermal parameters of each clothing layer are given in Tables 4a and 4b, respectively. Fig. 10 shows the measured data of Jones and Ogawa [23] and the predicted values of current model of sensible and latent heat loss to the environment from the clothed human body. On the same plot, Fu detailed human-clothing model results [17] are shown. When the cold fabric is suddenly exposed to hot environment at the same relative humidity, water vapor is adsorbed by the fabric

raising its temperature and hence reducing sensible heat loss from the clothed human body. The initial increase of fabric water vapor adsorption caused a decrease in latent heat loss to the environment. The initial response in hot exposure experiments is affected by the heat storage of the clothing leading to higher heat gain to the clothing surface than the heat gain to the skin. The current model simulation captures the transient effect and reproduces well the published experimental data of Jones and Ogawa and the data of the more detailed and complex model of Fu [17].

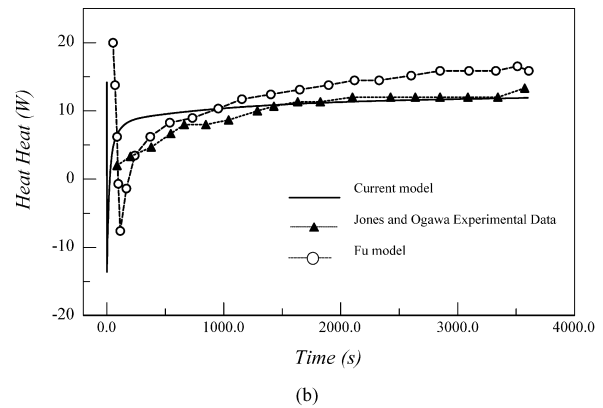
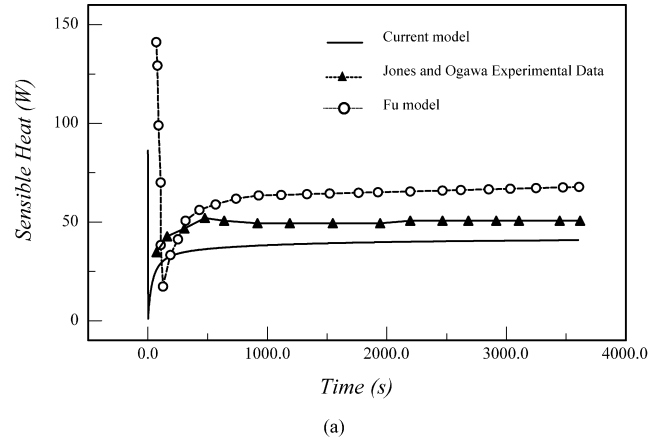


Fig. 10. The measured data of Jones and Ogawa [23], predicted values of current model and Fu Model [17] of (a) sensible heat gain; and (b) latent heat gain; in constant environment of 21.1 °C (70 F), 50% RH for a step change in temperature.

Table 4a

Fabric compositions for each clothing layer in Jones and Ogawa experiments [23]

Body element	First layer	Second layer	Third layer
Head	100% wool		
Chest	50% polyester 50% cotton	100% cotton	100% polyester
Pelvis	50% polyester 50% cotton	100% cotton	100% polyester
Left/right upper arm	50% polyester 50% cotton	100% cotton	100% polyester
Left/right fore arm	50% polyester 50% cotton	100% cotton	100% polyester
Left/right hand	100% wool		
Left/right thigh	50% polyester 50% cotton	50% polyester 50% cotton	
Left/right calf	50% polyester 50% cotton	50% polyester 50% cotton	
Left/right foot	100% cotton	100% leather	

Table 4b

Fabric properties for each clothing layer in Jones experiment [23]

Fabric composition	Thickness (mm)	Density (g m ⁻²)	Dry resistance (m ² °C W ⁻¹)	Evaporative resistance (m ² kPa W ⁻¹)	Specific heat (J kg °C)
100% Cotton	3.937	451.6	0.076	0.102	1210
50% Polyester 50% Cotton (first layer)	2.032	208.8	0.055	0.004	1275
50% Polyester 50% Cotton (second layer)	3.658	300.1	0.103	0.0106	1275
100% Polyester	30.513	247.6	0.379	0.055	1340
100% Wool (Hand)	4.674	611.1	0.114	0.02	1360
100% Wool (Head)	5.639	356.2	0.137	0.0236	1360
100% Leather	3.2	900	0.075	0.047	1430

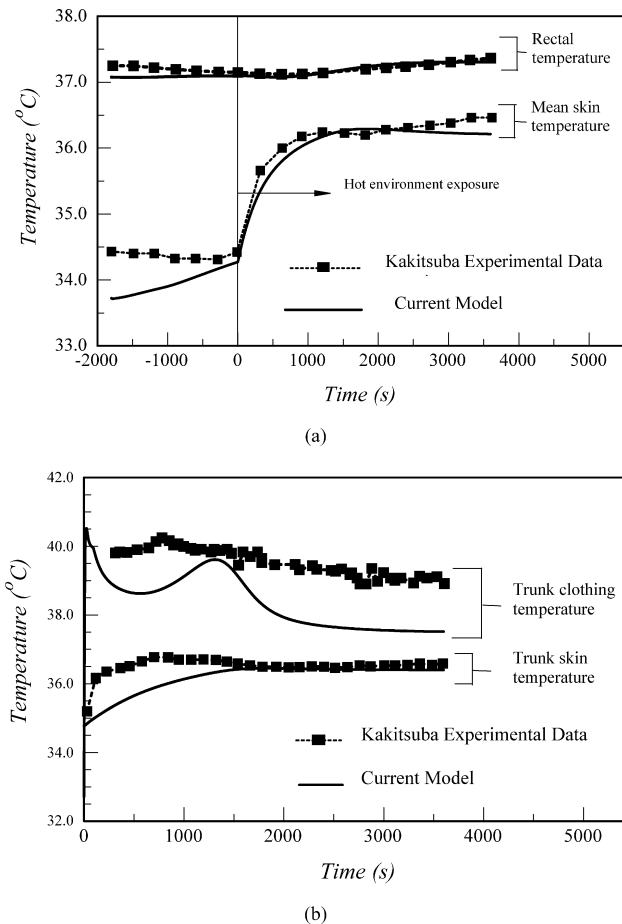


Fig. 11. The measured data of Kakitsuba [44] and predicted values of current model of (a) mean skin temperature and rectal temperature; and (b) trunk clothing and skin temperature; after one hour exposure to 40 °C/50% following exposure to 28 °C/50% RH for 30 minutes.

The second comparison of the clothed human model is performed against the experimental data reported by Kakitsuba [44]. No details about the clothing properties were reported except that they are made up of a 100% cotton T-shirt and a half short. The reported experiment protocol is similar to the one reported by Jones and Ogawa [23]. The experimental data were for subjects exposed to environment at 28 °C for a period of 30 minutes followed by a hot exposure to environment at 40 °C for a period of one hour. Kakitsuba reported rectal and mean skin temperatures for the duration of the experiment while the trunk and clothing temperatures were reported during the hot exposure period at 40 °C [1]. Fig. 11 shows the predicted (a) rectal and mean skin temperature and (b) the trunk skin and clothing temperatures by the current model and by the experimental results of Kakitsuba [44]. The predicted rectal temperature, mean skin temperature and trunk skin temperatures are found to be consistent with the experimental measurements. However, the predicted trunk clothing temperature is 1.5 °C lower than the experimental result which could be due to the use of lumped approximation for the clothing element. Under transient conditions, the outer most fabric temperature and pressure will be difficult to remain uniform. Water vapor adsorption under transient conditions due to water vapor accumulation in

the microclimate could cause the trunk clothing temperature to increase and then decrease approaching steady state condition. The model results show a similar increase/decrease in the trunk temperature to the experimental data of Kakitsuba [44] but with a delay of 3–4 minutes. Similar delays between experimental data and model were reported in literature [17] and attributed to the thermal load imposed by human test subjects when moving from pre-test condition chamber to the test chamber with a step change in temperature.

The current simple multi-node multi-segment bioheat model for nude and clothed human has shown good agreement with experimental data while using a realistic circulatory blood flow model. In addition to the initial thermal state of the human body, the metabolic rate is the main input parameter to the model that affects both the blood flow cardiac output, and the heat balances of each body segment. The model has produced accurate results that are comparable with recently published models results at a relatively lower computational cost and complexity. The model validations show that it can predict both core and skin temperatures for different body segments with reasonable accuracy under a range of environmental and exercise conditions (different metabolic rates).

5. Conclusion

A bioheat model is developed to predict human thermal responses in steady and transient conditions. The model has accurately simulated the human circulatory system and the perfusion blood flow rate in the core and skin layers that are used in the transient bioheat equations for the core, skin, and blood nodes in each body segment. The accuracy of the model is verified over a range of conditions for which it is applicable against published experimental data and other human body models simulation results. The model predicts well core, rectal, tympanic, and mean skin temperatures and the latent heat loss rate from the skin surface during heat and cold stress conditions and with reasonable accuracy during exercise and at rest.

Future work will extend the bioheat model to take into consideration non-uniform environment by incorporating angular variations of thermal response within the skin layer and clothing layers.

Acknowledgement

The authors would like to acknowledge the financial support of the University Research Board of the American University of Beirut.

References

- [1] A.P. Avolio, Multi-branched model of the human arterial system, *Med. Biol. Eng. Comp.* 18 (1980) 709–718.
- [2] C.K. Charney, Mathematical models of bioheat transfer, *Adv. Heat Transfer* 22 (1992) 19–155.
- [3] J.K. Choi, H.S. Lee, Y.S. Park, Effect of uniform and non-uniform skin temperature on thermal exchanges in water in humans, *Int. J. Biometeorol.* 47 (2003) 80–86.
- [4] C. Huizenga, Z. Hui, A model of human physiology and comfort for assessing complex thermal environments, *Build. Env.* 36 (2001) 691–699.

- [5] M. Salam, Experimental and numerical investigation of thermal comfort and energy consumption in spaces heated by radiant domestic stoves, Master thesis, American University of Beirut, 2004.
- [6] S. Tanabe, K. Kobayashi, J. Nakano, Y. Ozeki, M. Konishi, Evaluation of thermal comfort using combined multi-node thermoregulation (65MN) and radiation models and computational fluid dynamics (CFD), *Energy Build.* 34 (2002) 637–646.
- [7] A.P. Gagge, A two node model of human temperature regulation in FORTRAN, in: J.F. Parker, V.R. West (Eds.), *Bioastronautics Data*, second ed., Washington DC, 1973.
- [8] J.A.J. Stolwijk, J.D. Hardy, Temperature regulation in man: a theoretical study, *Pflügers Archiv. Ges. Physiology* 291 (1966) 129–162.
- [9] J.A.J. Stolwijk, Mathematical model of thermoregulation, in: *Physiological and Behavioral Temperature Regulation*, Charles C. Thomas Publishing Company, Illinois, 1970.
- [10] E.H. Wissler, Mathematical simulation of human thermal behavior using whole body models, in: *Heat. Mass Tran. Med. Biol.*, Plenum Press, New York, 1985.
- [11] X. Wang, Thermal comfort and sensation under transient conditions, PhD thesis, The Royal Institute of Technology, Stockholm, Sweden, 1994.
- [12] A.P. Gagge, Y. Nishi, An effective temperature scale based on a simple model of human physiological regulatory response, *ASHRAE. Trans. Part I* 77 (1971) 247–262.
- [13] C.E. Smith, A transient three-dimensional model of the thermal system, PhD thesis, Kansas State University, 1991.
- [14] P.O. Fanger, *Thermal Comfort, Analysis and Applications in Engineering*, McGraw-Hill, New York, 1982.
- [15] D. Fiala, K.J. Lomas, M. Stohrer, Computer predictions of human thermoregulatory and temperature responses to a wide range of environment conditions, *Int. J. Biometeorol.* 45 (2001) 143–159.
- [16] H.H. Pennes, Analysis of tissue and arterial blood temperature in the resting human forearm, *J. Appl. Phys.* 1 (1948) 93–102.
- [17] G. Fu, A transient 3-D mathematical thermal model for the clothed human, PhD thesis, Kansas State University, 1995.
- [18] P.S.H. Henry, Diffusion in absorbing media, *Proc. Roy. Soc. A* 171 (1939) 215–241.
- [19] P. Nordan, H.G. David, Coupled diffusion of moisture and heat in hygroscopic textile fabrics, *Int. J. Heat Mass Transfer* 10 (1967) 853–866.
- [20] Y. Li, B.V. Holcombe, A two stage sorption model of the coupled diffusion of moisture and heat in wool fabrics, *Textile Res. J.* 62 (1992) 211–217.
- [21] B. Farnworth, A numerical model of combined diffusion of heat and water vapor through clothing, *Textile Res. Inst.* 56 (1986) 653–655.
- [22] B.W. Jones, Accurate modeling of heat and mass transport from the human body, in: *33rd Thermophysics Conference*, Kansas State University, 1999.
- [23] B.W. Jones, Y. Ogawa, Transient interaction between the human and the thermal environment, *ASHRAE Trans.* 98 (1993) 189–195.
- [24] A. Shitzer, R.C. Eberhart, *Heat Transfer in Medicine and Biology: Analysis and Applications*, Plenum Publishing Corporation, 1985.
- [25] J.C. Chato, Heat transfer to blood vessels, *J. Biomech. Eng.* 102 (1980) 110–118.
- [26] W.R. Milnor, *Hemodynamics*, second ed., Williams and Wilkins, 1989.
- [27] S. Weinbaum, L. Jiji, Theory and experiment for the effect of vascular temperature on surface tissue heat transfer – Part 1: anatomical foundation and model conceptualization, *ASME J. Biomech. Eng.* 106 (1984) 246–251.
- [28] C.J. Schwartz, N.T. Werthessen, S. Wolf, *Structure and Function of the Circulation*, 1, Plenum Press, New York, 1980.
- [29] W.W. Nichols, M.F. O'Rourke, *McDonald's Blood Flow in Arteries*, fourth ed., Arnold Editions, 1998.
- [30] *ASHRAE, Handbook of Fundamentals*, American Society of Heating, Refrigerating and Air Conditioning Engineers, Atlanta, 2001.
- [31] R. Gordon, A mathematical model of the human temperature regulatory system – transient cold exposure response, *IEEE Trans. Biomed. Eng.* 23 (1976).
- [32] J.R. Womersley, An elastic tube theory of pulse transmission and oscillatory flow in mammalian arteries, *Aeronautical Research Laboratory, WADC Technical Report*, 1957, pp. 56–614.
- [33] F.R. Valentin, *Hurst's the Heart*, eleventh ed., McGraw-Hill, 2005, <http://www.accessmedicine.com>.
- [34] O.I. Craciunescu, S.T. Clegg, Pulsatile blood flow effects on temperature distribution and heat transfer in rigid vessels, *ASME J. Biomech. Eng.* 123 (2001) 500–505.
- [35] Z. Guo, H.J. Sung, Analysis of Nusselt number in pulsating pipe flow, *Int. J. Heat. Mass Tran.* 40 (1997) 2486–2489.
- [36] G. Havenith, Individualized model of human thermoregulation for the simulation of heat stress response, *J. Appl. Phys.* 90 (2000) 1934–1954.
- [37] B.W. Jones, Non-steady state heat and mass transfer in fabrics, in: *Proceedings of the International Symposium on Fiber Science and Technology*, Yokohama, 1994.
- [38] W.E. Mortan, L.W. Hearle, *Physical Properties of Textile Fibers*, Heinemann, London, 1975.
- [39] C.J. Mills, I.T. Gabe, J.H. Gault, P.T. Mason, J. Ross, E. Braunwald, Pressure-flow relationships and vascular impedance in man, *Cardiovascular Res.* 4 (1970) 405–416.
- [40] W.F. Ganong, *Review of Medical Physiology*, eleventh ed., LANG Medical Publications, Los Altos, California, 1983.
- [41] J.D. Hardy, J.A.J. Stolwijk, Partitioned calorimetric studies of man during exposures to thermal transients, *J. Appl. Phys.* 21 (1966) 967–977, 1799–1806.
- [42] P.R. Raven, S.M. Horvath, Variability of physiological parameters of unacclimatized males during a two-hour cold stress of 5 °C, *Int. J. Biometeorol.* 14 (1970) 309–320.
- [43] B. Saltin, L. Hermansen, Esophageal, Rectal and muscle temperature during exercise, *J. Appl. Phys.* 21 (1966) 1757–1762.
- [44] N. Kakitsuba, Dynamic changes in sweat rates and evaporation rates through clothing during hot exposure, *J. Therm. Biol.* 29 (2004) 739–742.